(2)

OFFICE OF NAVAL RESEARCH

GRANT NO. N00014-91-J-1447
R&T CODE 414044

Technical Report No. 32



# THERMODYNAMIC AND KINETIC ASPECTS OF III/V EPITAXY

by

G. B. STRINGFELLOW

Prepared for Publication

in the

Proceedings of Croissance de cristaux et de couches epitaxiales a applications electroniques et optiques

University of Utah
Dept. of Materials Science & Engineering
Salt Lake City, UT 84112

May 22, 1992

# THERMODYNAMIC and KINETIC ASPECTS OF III/V EPITAXY

G.B. Stringfellow
University of Utah
Salt Lake City, Utah 84112

## ABSTRACT

Crystal growth processes in general and epitaxial processes in particular are often discussed in terms three disciplines: thermodynamics, mass transport and hydrodynamics, and chemical reaction kinetics. This paper will concentrate on two of these, the thermodynamic and kinetic aspects of epitaxy. Three major influences of thermodynamics will be discussed: 1) Thermodynamics defines the driving force and hence the upper limit of growth rate. This occurs only when all reactants in the system are allowed to equilibrate with the substrate. 2) Thermodynamics often controls stoichiometry and the solid composition of alloys. An understanding of thermodynamic and kinetic constraints can lead to the growth of metastable alloys. 3) The driving force for ordering into natural superlattice structures during growth is also governed by thermodynamics. The actual ordered structures observed are dependent on the surface kinetics. This aspect of kinetics will be addressed in addition to the kinetics of both homogeneous and heterogeneous chemical reactions occurring during growth. Each of these topics is addressed in terms of fundamental concepts, with examples from recent research on the epitaxial growth of III/V semiconductor compounds and alloys.

## 1. INTRODUCTION

All epitaxial growth processes are highly complex. Indeed, early crystal growth studies were largely empirical, giving crystal growth the appearance of an art. This is partly because of the complex, multicomponent, multiphase systems that are normally of interest, and partly because the process is dynamic and inhomogeneous phases are inherent. In an effort to systematically study and understand such a complex situation the fundamental processes occurring during crystal growth are commonly subdivided into hydrodynamics and mass transport, the kinetics of chemical reactions occurring homogeneously in the gas phase and heterogeneously at the surface, and thermodynamics. Thermodynamic aspects of crystal growth are in many ways the most important. This especially true when the growth rate is very slow. At low growth rates and relatively high temperatures, the chemical reaction kinetics play less of a role than in very rapid crystal growth processes. In the limit of infinitely slow growth rates thermodynamics defines the concentrations in the two phases typically present during epitaxial growth. Thermodynamics also acts as the driving force for any crystal growth process, hence defining the maximum growth rate. Thermodynamics is also able to predict solid composition for many growth conditions. This includes not only alloy composition, but also solid stoichiometry, incorporation of impurities, separation into several solid phases, and the occurrence of ordered superlattice structures in the solid. Thus, the thermodynamic aspects of epitaxy must be understood before proceeding to kinetic aspects of growth which frequently control growth rate and certainly affect solid composition, the phases appearing, and the occurrence of ordering

in many situations. More and more, the understanding of the basic aspects of epitaxy has allowed a departure from the empirical approach to crystal growth.

The fundamentals of thermodynamics will be reviewed first . Examples, taken mainly from the author's work in the area of organometallic vapor phase epitaxial (OMVPE) growth of III/V alloys, will be used to illustrate the important concepts. However, the concepts are general and apply to all epitaxial processes. This will form the background for a discussion of the kinetic aspects of epitaxy, including homogeneous and heterogeneous chemical reactions as well as the physical processes occurring on the surface during epitaxial growth.

## 2. THERMODYNAMIC TREATMENT OF VPE

The equilibrium state for a two phase, $\alpha + \beta$, system is defined in terms of the chemical potentials,

$$\mu_i^{\alpha} = \mu_i^{\beta} , \qquad (1)$$

where the subscript i indicates the ith component and the superscripts indicate the phase. The chemical potential is usually written in terms of the chemical potential in an arbitrary standard state, denoted by the superscript zero,

$$\mu = \mu^o + RT \ln p/p^o . \qquad (2)$$

For an ideal gas mixture,

$$\mu_i = \mu_i^o + RT \ln p_i/p_i^o , \qquad (3)$$

where $p_i$ is the partial pressure, equal to the mole fraction $x_i$ multiplied by P, the total pressure, and the standard state is usually pure component i.

For an ideal liquid or solid solution, the same expression holds with $p_i/p_i^o$ replaced by $x_i/x_i^o$. However, the standard state is pure i, so $x_i^o = 1$. The form of eq. (3) is so useful that it is retained even for non-ideal solutions with $x_i$ replaced by the activity, $a_i$, which may also be considered a product of $x_i$ multiplied by a non-ideality factor, $\gamma_i$, the activity coefficient.

### 2.1 Driving Force for Epitaxy

For the OMVPE growth of GaAs using trimethylgallium (TMGa) and arsine ($AsH_3$) the overall reaction is,

$$(CH_3)_3Ga(v) + AsH_3(v) = GaAs(s). \qquad (4)$$

Assuming the TMGa and $AsH_3$ to completely decompose in the gas phase to give Ga and $As_4$, an assumption to be revisited in the discussion of kinetics, below, the reaction can be simplified:

$$Ga(v) + 1/4\ As_4(v) = GaAs(s). \qquad (5)$$

The equilibrium condition is

$$\mu^v_{Ga} + 1/4\ \mu^v_{As} = \mu^s_{GaAs}, \qquad (6)$$

or

$$\mu^{ov}_{Ga} + 1/4\ \mu^{ov}_{As} + RT \ln p^e_{Ga} p^e_{As} = \mu^{os}_{GaAs} + RT \ln a_{GaAs}, \qquad (7)$$

where the superscript "e" denotes the equilibrium value of partial pressure. Thus,

$$a_{GaAs} / p^{e}_{Ga}\, p^{e}_{As} = K_{GaAs}, \quad (8)$$

where K is the equilibrium constant. This is the basic law of mass action.

When the system is not at equilibrium, the thermodynamic driving force to restore equilibrium is

$$\Delta\mu = \mu^{v}_{Ga} + 1/4\, \mu^{v}_{As} - \mu^{s}_{GaAs}, \quad (9)$$

or

$$\Delta\mu = RT \ln (p_{Ga} p_{As} / p^{e}_{Ga} p^{e}_{As}). \quad (10)$$

This is the driving force for epitaxy. A situation is intentionally created where higher than equilibrium reactant vapor pressures drive the system to produce the GaAs solid desired. The maximum quantity of GaAs solid that can be produced is simply the amount (the supersaturation) that would establish equilibrium and is thus fundamentally limited by thermodynamics and the total amount of gas transported through the VPE reactor. Similar reasoning can be applied to any of the vapor phase growth processes as well as to liquid phase epitaxy (LPE).

The thermodynamic driving forces for the various epitaxial processes vary enormously. The LPE technique is widely regarded as occurring under near-equilibrium conditions. Of course, no system having a continuous change from liquid or vapor to solid can be at equilibrium. However, for the LPE growth of GaAs with a typical supercooling of <10K, the thermodynamic driving force can be calculated to be <200 cal/mol. This is a useful basis of comparison with other techniques. The hydride vapor phase epitaxial (HVPE) and chloride VPE (ClVPE) techniques (for a description of the various epitaxial processes, refer to the following paper) are also sometimes regarded as near-equilibrium techniques, since reversible processes occur at the interface due to the volatility of both the group III chlorides and the group V dimers and tetramers. However,

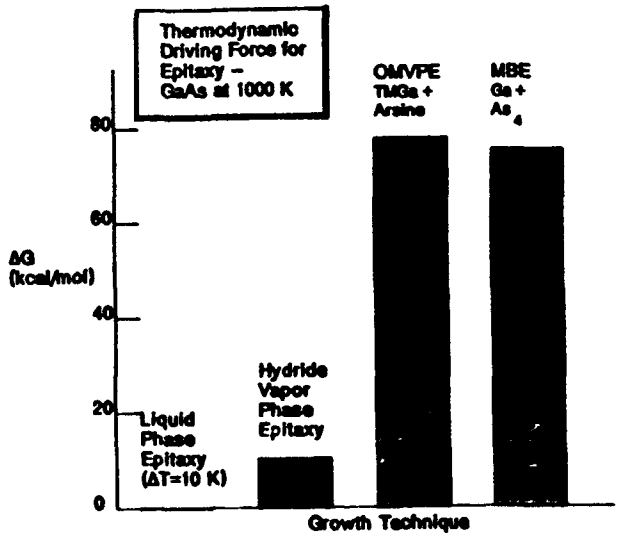


Fig. 1. Estimated thermodynamic driving force, Gibbs free energy difference between reactants and products, for several epitaxial growth processes. All calculations are for the growth of GaAs at 1000 K. (after Stringfellow[31]).

as shown in Fig. 1, the thermodynamic driving force for the HVPE growth of GaAs at 1000 K is orders of magnitude larger than for LPE. This is partly because of the instability of arsine at this temperature. Nevertheless, a near equilibrium condition may exist at the interface. Thus, for many growth conditions, thermodynamic calculations give a good description of the dependence of solid composition on the vapor composition and growth temperature for both HVPE and ClVPE[1]. The situation is even more dramatic for OMVPE growth using arsine and TMGa, the process described above. As is seen in Fig. 1, the thermodynamic driving force is significantly greater than for HVPE. This is due to the instability of the TMGa at 1000 K: Both reactants are initially in very high free energy states. Thermodynamics also gives a good description of solid composition in this system[2]. The supersaturation is also extremely high for molecular beam epitaxy (MBE), where, at high temperatures, the III/V semiconductor is much more stable than the elements in the vapor phase. Nevertheless, thermodynamics is a powerful tool in analyzing MBE growth[3].

Ordinarily, in any VPE system, the growth rate is considerably less than that calculated from thermodynamics. Kinetics, both surface reaction rates (at low temperatures) and diffusion through the gas phase (at higher temperatures), are not rapid enough to allow equilibrium to be established throughout the system at all times. This situation is illustrated by Fig. 2a, where $\Delta\mu$ from eq. (9) is

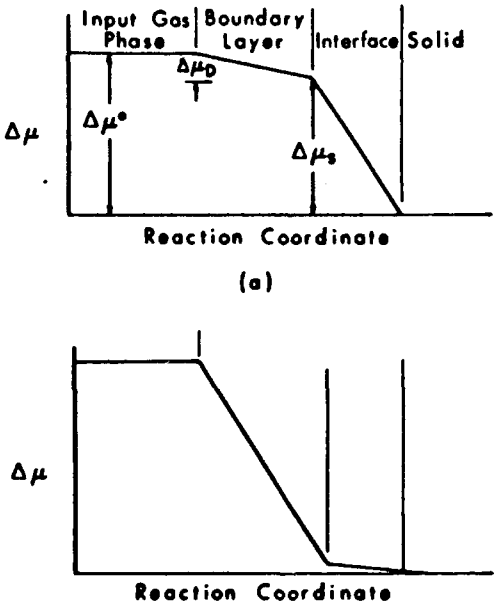


Figure 2. Schematic diagram of chemical potential versus reaction coordinate, showing the drop in chemical potential required for each step in the growth sequence to keep all rates equal. The differences in individual chemical potentials can alternatively be thought of as ratios of partial pressures of the reactants: a) the general case (After Stringfellow[32]) and b) the case of rapid surface kinetics, i.e., with $\Delta\mu_S << \Delta\mu_D$ (After Stringfellow [33]).

plotted versus reaction coordinate. This allows the schematic representation of the overall, thermodynamic driving force for the growth reaction, represented as $\Delta\mu^*$. The superscript "* " denotes the chemical potential in the input gas phase, where for all reactants $p_i = p^*_i$. The growth rate is proportional to the flux of atoms diffusing through the boundary layer, which is identical to the flux of atoms crossing the interface into the solid. The diagram shows schematically the driving forces necessary to sustain this flux for the diffusion process ($\Delta\mu_D$) and the surface reactions ($\Delta\mu_S$).

Even in cases with a large supersaturation in the input vapor phase, i.e., $\Delta\mu^* >> 0$, near equilibrium conditions may exist at the growing solid surface. This simply requires that the interface kinetics be much more rapid than the diffusion kinetics, i.e., the two processes proceed at the same rate with $\Delta\mu_S << \Delta\mu_D$. This situation, termed diffusion limited growth, is shown schematically in Fig. 2b. Using ordinary growth conditions, with temperatures between approximately 550 and 800 C, this is the normal situation for the OMVPE growth of GaAs, as deduced from the nearly temperature independent growth rate, as seen in Fig. 3. For surface kinetically limited processes, the growth rate increases exponentially with increasing temperature[4,5]. This occurs for the OMVPE growth of GaAs at temperatures below approximately 550 C when TMGa is the Ga precursor, but this temperature depends on the group III precursor used, as discussed below.

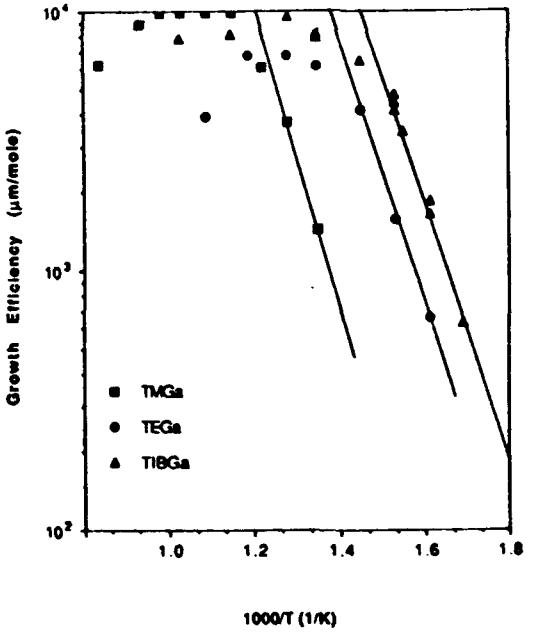


Figure 3. Growth efficiency (growth rate/group III molar flow rate) versus reciprocal temperature for various Ga alkyls: TMGa (■), TEGa (●), and TIBGa (▲). (After Stringfellow[34]). The data are from Plass et al[38].

In the diffusion limited case, illustrated schematically in Fig. 2b, the interfacial partial pressures, $p^i_i$, nearly satisfy the equilibrium relationship,

$$a_{GaAs}/ p^i_{Ga}\, p^i_{As} = K_{GaAs}. \quad (11)$$

Since the input vapor is highly supersaturated,

$$p^*_{Ga}\, p^*_{As} >> p^i_{Ga}\, p^i_{As}. \quad (12)$$

This is equivalent to stating that $\Delta\mu^*>>0$. For the typical case

$$p^*_{Ga} << 4p^*_{As}, \quad (13)$$

i.e., the V/III ratio is >>1, as will be discussed in a later section. This means that the Ga is nearly depleted at the interface,

$$p^i_{Ga} << p^*_{Ga}, \quad (14)$$

while the $As_4$ partial pressure is hardly diminished,

$$p^i_{As} \approx p^*_{As}, \quad (15)$$

since the same number of As and Ga atoms are removed from the vapor phase to produce GaAs. This situation makes the analysis of growth rate and solid composition particularly simple.

The growth rate is proportional to the flux of Ga and As atoms through the boundary layer of thickness d. The two fluxes are equal, since stoichiometric GaAs is the only product. The flux may be expressed,

$$J = D_{Ga}(p^*_{Ga} - p^i_{Ga})/RTd, \quad (16)$$

where $D_{Ga}$ is the diffusion coefficient of Ga, in whatever form it may appear while diffusing through the boundary layer. In light of eq. (14), the Ga flux and the GaAs growth rate are proportional to $p^*_{Ga}$, as observed experimentally[5]. Equally clear is that the ratio of the concentrations of A and B for alloys with mixing on the group III sublattice, $A_{1-x}B_xC$, will be the same as the ratio $p^*_A/p^*_B$, assuming the diffusion coefficients for the A and B species are nearly the same[6,7].

## 2.2 Solution Thermodynamics

The condition for thermodynamic equilibrium is expressed by eq. (1) and the discussion at the beginning of Section 2. Using these concepts, applied to the solid-vapor equilibria of concern for VPE, and the liquid-solid equilibria for LPE, we can calculate the composition of a multicomponent solid alloy from the temperature and the concentrations of the various components in the nutrient phase. Deviations from ideality for the vapor phase are commonly neglected. However, non-ideality in the solid and liquid phases must be considered. For the nearly-metallic liquids used for LPE, the liquid is described by the "regular solution" model[8]. Fortunately, for semiconductor systems the solid can often be described using either the regular solution or "delta-lattice-parameter" (DLP)[9] models. In both cases the distribution of elements on a sublattice is considered to be random, thus the entropy of mixing for a pseudobinary solution of the type $A_{1-x}B_xC$ is simply the ideal configurational entropy of mixing,

$$\Delta S^M = -R[x \ln x + (1-x) \ln(1-x)]. \quad (17)$$

For the regular solution model, the enthalpy of mixing is obtained by summing nearest-neighbor bond energies, yielding,

$$\Delta H^M = x(1-x)\,\Omega^s, \qquad (18)$$

where $\Omega^s$ is the interaction parameter. The activity coefficient may be written,

$$\ln\gamma_i = (1-x_i)^2\Omega/RT. \qquad (19)$$

Physically, the regular solution model cannot provide an accurate, predictive description of the enthalpy of mixing in semiconductor alloys. However, simple models developed to interpret the band gap and optical properties can be used to treat the bonding in semiconductor alloys.[9] The DLP model allows accurate calculation of $\Omega^s$ in terms of the difference in lattice parameters between AC and BC:

$$\Omega^s = 5\times10^7\,(a_{AC} - a_{BC})^2[(a_{AC} + a_{BC})/2]^{-4.5}. \qquad (20)$$

This first-order treatment of the enthalpy of mixing is apparently equivalent to simply the strain energy caused by the lattice parameter difference. The solutions are predicted to be ideal for alloys from compounds with the same lattice constant such as GaAs and AlAs, and to have positive deviations from ideality for all other alloys. The DLP model predicts a large positive enthalpy of mixing for systems with a large difference in lattice constant. This can overwhelm the negative configurational entropy of mixing for temperatures below the critical temperature, $T_c$, resulting in a free energy versus composition curve with an upward bowing in the center. This dictates that at equilibrium a random alloy in a certain composition range will decompose into a mixture of two phases, i.e., the phase diagram contains a miscibility gap.

The equilibrium conditions for the ternary(or pseudobinary) system may be obtained in exactly the same way as described for binary systems in section 2.1, by equating the chemical potentials of the 2 components in the 2 phases:

$$\mu^v_A + \mu^v_C = \mu^s_{AC}, \qquad (21a)$$

$$\mu^v_B + \mu^v_C = \mu^s_{BC}. \qquad (21b)$$

This leads to two mass action expressions, similar to eq. (11). As discussed in section 2.1, equilibrium is assumed to be established at the interface. Such calculations have been applied to many alloy systems for HVPE, CIVPE, and OMVPE systems, as well as for LPE and MBE with excellent results. For LPE, the calculations result in well-known liquid-solid phase diagrams[2,9].

As an example of the use of such calculations to understand epitaxial processes, consider the OMVPE growth of $GaAs_{1-x}Sb_x$. The 2 mass action expressions, one for GaAs and one for GaSb, are solved simultaneously with 2 conservation equations, one for solid stoichiometry and one for solid composition[10]. Complete pyrolysis of the source molecules is normally assumed. This assumption is incorrect for very stable molecules at all temperatures and for all molecules at very low temperatures, as will be discussed below in the Kinetics Section. The activity coefficients of GaAs and GaSb in the solid are calculated as described above using the DLP model.

The calculation can be performed with no adjustable parameters, yielding solid composition versus vapor composition and substrate temperature during growth. The calculated results are compared with experimental data in Fig. 4.

Several important aspects of VPE are illustrated in this rather complex figure. First, consider the open data points, obtained for an input V/III ratio (the ratio of the input group V to group III molar flow rates) of 2.0. Notice that the calculated curve for V/III = 2.0 fits the data well. The Sb distribution coefficient, defined as $k_{Sb} = x^{S}_{Sb}/x^{V}_{Sb}$, where $x^{V}_{Sb} = p^{*}_{TMSb}/(p^{*}_{TMSb}+p^{*}_{AsH})$, is seen to be less than unity. GaAs is more stable than GaSb, thus As is more likely to bond to the Ga on the surface and be incorporated into the solid. The excess Sb evaporates from the surface. An additional important point is that the calculation for a V/III ratio of less than unity yields an antimony distribution coefficient of unity. As discussed in section 2.1 for the case of alloys with mixing on the group III sublattice, when V/III>1, essentially all of the group III elements reaching the interface are incorporated. The case of GaAsSb with mixing on the group V sublattice with V/III<1 is completely analogous. The establishment of equilibrium at the interface while the input vapor is highly supersaturated requires that the group V elements be virtually exhausted at the interface. A final point relative to Fig. 4 is the presence of a two solid phase region or miscibility gap. Because of the large difference in lattice constant between GaAs and GaSb a miscibility gap exists[11]. However, when the V/III ratio is less than unity, the As and Sb atoms arriving in a random pattern at the surface do not have time to redistribute themselves into GaAs and GaSb rich areas before being covered over by the next layer. Thus, we are able to grow metastable $GaAs_{1-x}Sb_x$ alloys throughout the entire range of solid composition as shown by the solid data points in Fig. 4. Other, even less stable alloys, such as GaPSb and InPSb can also be grown in this way[12].

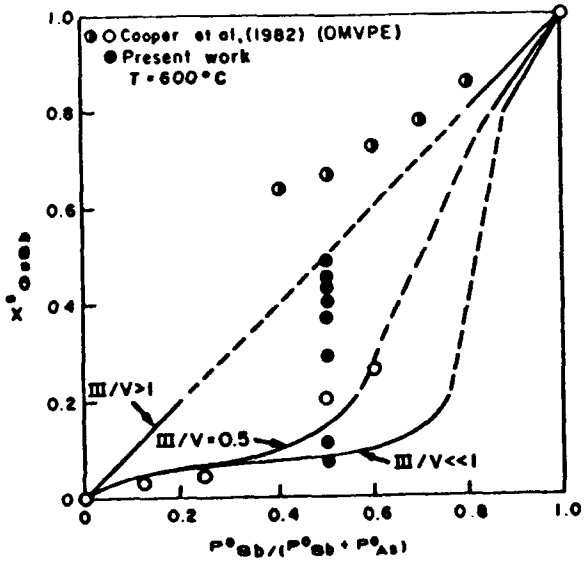


Figure 4. Solid versus vapor composition for the alloy $GaAs_{1-x}Sb_x$. The data are from the work of Cooper et al[35] for V/III = 2.0(○), and V/III = 0.5(◐), and the work of Stringfellow and Cherng[36](●). The curves were calculated for various V/III ratios. The broken sections of each curve represent the calculated regions of solid immiscibility. (After Stringfellow and Cherng[36]).

## 2.4 Solid Phase Immiscibility

For GaAsSb, the value of $T_c$ is approximately 745 C[10]. At typical growth temperatures, the solid compositions inside the miscibility gap, which covers nearly the entire composition range, cannot be grown by LPE[13]. We have already discussed the ability to grow the metastable alloys by OMVPE. They can also be grown by molecular beam epitaxy (MBE)[14]. Recently, it has been discovered that these alloys may also exhibit an ordered, superlattice structure[15]. This is indicated by extra, zincblende-forbidden {100} and {1,1/2,0} spots in the electron diffraction patterns, indicating that the solid is ordered, with two separate ordered structures.

Ordering in a thermodynamic system where the random alloy exhibits a large positive enthalpy of mixing is not possible for a regular solution[8], another indication that this model is not physically appropriate for III/V semiconductor alloys. Interestingly, the driving force for ordering is a reduction of strain energy, the same factor which leads to a large positive enthalpy of mixing. The ordered structures are able to accommodate the two dissimilar bond lengths when $\Delta a \neq 0$ with a minimum of distortion.

Ordering has now been observed in essentially all III/V alloys grown by OMVPE and MBE[16]. The {111} ordered structure (Cu-Pt) with 4 variants, corresponding to the 4 crystallographic distinct {111} planes in a cubic lattice, is normally observed for III/V alloys. Only 2 are observed during OMVPE growth for (001)-oriented substrates. This is apparently due to the lower symmetry of a reconstructed, As-rich surface. For growth systems where reconstruction is believed absent, such as LPE, no ordering occurs. These and other phenomena indicate that the ordering phenomena cannot be totally explained by thermodynamic factors: Kinetic factors appear to be important.

# 3. KINETICS

## 3.1. Motion of Surface Steps

Surface analytical techniques that can be applied during MBE growth have given considerable information about the atomic configurations on semiconductor surfaces under various conditions. The unreconstructed As-rich (001) GaAs surface consists of As atoms forming only two bonds to underlying Ga atoms. The two dangling bonds per surface atom give this configuration a very high energy. The energy is reduced dramatically by the formation of dimers between adjacent As atoms[17]. These dimers run in [110] rows on the surface. An atom being attached to a kink moving along the step, the process leading to growth, thus sees two types of sites[18]. One involves the formation of bonds to the underlying lattice atoms and the other also involves the formation of a dimer bond. In addition, the location of the dimers is correlated to the size of the underlying atoms. These two factors give rise to the formation of 2 particular variants of the Cu-Pt structure during growth on (001)-oriented substrates[16,18]. The model correctly predicts the formation of the same two variants for both alloys with mixing on the group III sublattice, such as GaInP, and for those with mixing on the Group V sublattice, such as GaAsP[16,18]. The model also predicts that the direction of [110] step motion will determine which

of the two variants will be formed. This is dramatically confirmed by recent experiments where the direction of step motion has been controlled by patterning the surface with [110]-oriented grooves[18-20]. The GaInP grown on the two sides of the groove is produced by the motion of steps in opposite directions. This results in each half of the groove being filled by a single domain, consisting entirely of a material ordered with the same variant of the Cu-Pt structure. Similar, but slightly more complex, results have also been obtained for GaAsP[20]. This is a dramatic demonstration of the control of ordering. These are the first macroscopic domains ever produced. The cross sectional size is 1/2 the groove width by the layer thickness. The length is the dimension of the substrate, i.e., the length of the groove.

## 3.2 CHEMICAL REACTIONS

The effects of chemical kinetics are invariably observed during epitaxial growth when the rates of the chemical reactions necessary for growth are slower than the mass transport rates. Thus, the growth rate falls off at low temperatures, as seen in Fig. 3 and discussed above. By comparing the temperature dependence of GaAs growth rates for several Ga precursors, as in Fig. 3, we observe that the pyrolysis of the group III precursor is the rate determining step, not surprising since the V/III ratio is typically much greater than unity. TMGa, with the highest radical-Ga bond strength, gives the lowest growth rate. The Ga-ethyl bond strength is lower, resulting in a higher growth rate for triethylgallium (TEGa). The precursor with the lowest bond strength, triisobutylgallium (TIBGa), gives the highest growth rates at low temperatures. This is an excellent example of the interconnection between the details of pyrolysis of the precursor and growth results. The practical consequence is that efficient low temperature growth can only be accomplished by designing group III precursors with lower bond strengths.

Only recently have the details of the reactions for pyrolysis of the group III and group V precursors, alone and in combination, been studied. The chemical reactions occurring during growth differ tremendously for the various vapor phase growth techniques. They range from solely group V tetramer-dimer-monomer reactions for MBE[21] to complex radical reactions occurring both in the gas phase and on the surface for OMVPE. This is perhaps the most complex and least experimentally accessible aspect of vapor phase growth. Two approaches have been adopted to study these processes: 1) The study of chemical reactions using analytical techniques such as infrared spectroscopy and mass spectroscopy, either by sampling the exhaust or by in-situ sampling. 2) The study of surface chemical reactions using sophisticated surface analytical techniques that are normally applied only in UHV chambers. Each approach will be discussed briefly.

Perhaps the simplest approach to studying both homogeneous and heterogeneous chemical reactions involves the use of a mass spectrometer to sample the effluent gas from an ersatz reactor, an isothermal flow-tube reactor[22]. This approach has the advantage of yielding data from which rate constants can be determined. The disadvantage is that intermediate species cannot be detected. Thus, the reaction mechanisms can only be determined by

a combination of sophisticated techniques including the use of isotopic labelling of the reactants, the comparison of reaction rates and products in He, $H_2$, and $D_2$ ambients, the addition and removal of radicals from the system, and the use of various times, temperatures, and reactant concentrations. While it can never be claimed that the reaction mechanism has been unequivocally determined, the results and consequent pyrolysis models may be useful guides to the design of both the experimental conditions to be used for OMVPE growth as well as the precursor molecules, themselves.

The only example of this approach considered here will be a brief examination of the pyrolysis of the novel, non-hydride phosphorus precursor tertiarybutylphosphine (TBP). Simply determining the percent decomposition versus temperature for a fixed reaction time but with variable input TBP concentrations reveals that the pyrolysis process is not unimolecular, since the decomposition rate increases with increasing reactant concentration[23]. The products obtained versus reactor temperature for various input concentrations, are shown in Fig. 5. They clearly indicate that several reactions are occurring in parallel, since the product is mainly $C_4H_8$ for low input TBP concentrations and $C_4H_{10}$ at higher concentrations. From the product distribution a hypothetical reaction scheme can be suggested, namely that $C_4H_8$ is produced by the two sequential unimolecular reactions (22) and (23), below, and that $C_4H_{10}$ is produced by radical attack of the parent molecule, removing an H atom, the 2nd order reaction (24).

$$C_4H_9PH_2 \rightarrow C_4H_9 + PH_2 \qquad (22)$$

$$C_4H_9 \rightarrow C_4H_8 + H \qquad (23)$$

$$C_4H_9PH_2 + C_4H_9 \rightarrow C_4H_9PH + C_4H_{10} \; . \qquad (24)$$

The rate of the second order reaction, producing $C_4H_{10}$, increases more rapidly as the input concentration increases than the rates of the first order reactions (22) and (23). Since a number of other models would give similar results, the hypothetical model has been tested by using[24] deuterated $TBPd_2$. The dominant product at high concentrations becomes $C_4H_9D$, supporting the proposed model. To further test the proposed mechanism, $C_4H_9$ radicals were added to the system[25] by adding azo-t-butane (ATB) a compound that pyrolyzes yielding 2 t-butyl radicals and inert $N_2$ at temperatures below those required for the onset of reaction (22). The temperature for the onset of TBP pyrolysis is dramatically reduced and now coincides with that for ATB. Clearly the t-butyl radicals cause the pyrolysis of TBP. Thus, the indirect evidence, taken together, makes a convincing case that TBP pyrolysis occurs mainly via reactions (22-24). The pyrolysis mechanism for TBAs may be similar, since ATB has been demonstrated to have a similar effect on the pyrolysis rate[25].

Understanding the pyrolysis processes for the individual precursors is directly relevant to understanding and controlling the vapor phase growth techniques. As an example, consider the growth of GaAs and GaP using TMGa plus either TMAs or TBP. The results of systematic studies of the interactions between

TMGa and TBP indicate that the $PH_2$ radicals generated during TBP pyrolysis [reaction (22)] attack TMGa on the semiconductor surface, enhancing their pyrolysis rate by removing $CH_3$ radicals[24,26]. This is also an important process for removing methyl radicals from the system, resulting in a reduction in carbon contamination. Recent results for GaAs grown using TMGa demonstrate TBAs pyrolysis probably also generates $AsH_2$ radicals.

The chemical reactions occurring specifically at the semiconductor surface have been studied fairly intensively by using UHV surface spectroscopic probes developed for the study of catalysis, such as electron diffraction, photoemission, Auger electron spectroscopy, electron energy loss spectroscopy, thermally programmed desorption, and modulated beam mass spectroscopy (MBMS)[28,29]. The elementary processes involved in UHV growth techniques, chemical beam epitaxy(CBE) for example, such as the heterogeneous pyrolysis of TEGa, have been the subject of dozens of studies within the last few years. Such studies have the advantage of simplicity. Thus, they may give more direct, less ambiguous information about chemical reactions than the more complex experiments described above for combined group III and group V precursors in a flowing, atmospheric-pressure ambient. Nevertheless, the

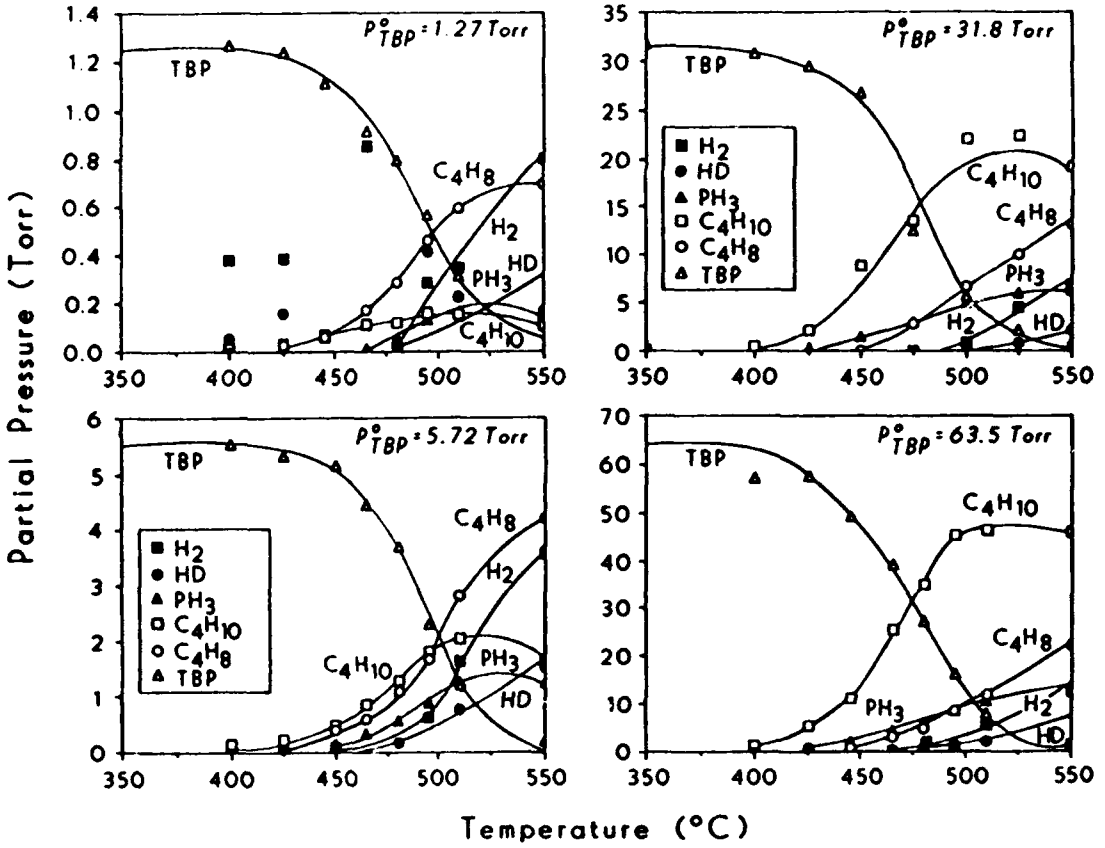


Figure 5. Products of TBP decomposition versus temperature for several initial TBP concentrations. (After Li et al[37]).

experimental conditions are frequently very dissimilar to those used for growth, even under UHV conditions where gas phase collisions do not occur. The times involved are frequently very different than those important for growth processes. In addition, the species on the surface may interact during growth. Thus, having a specific surface coverage of a single species, although convenient experimentally, may reveal little about the actual processes occurring during epitaxial growth where the surface coverage may be much different. The most meaningful experiments are probably those involving the simultaneous presence of both group III precursors, such as TEGa, TMGa, or trimethylindium (TMIn), and group V molecules, such as As dimers and/or tetramers.

Using these surface probes, the complex dependence of growth rate on temperature for TEGa combined with $As_2$ has been carefully studied and modelled. Martin and Whitehouse[28] have devised the following scheme based on their MBMS studies. As expected, at very low temperatures, TEGa does not pyrolyze. At temperatures up to 350°C, DEGa is formed, but desorbs without further decomposition. Thus, the growth rate remains nearly zero. As the temperature is increased above 350°C, the growth rate increases, since the pyrolysis can now proceed to elemental Ga. However, a progressive decrease in growth rate is observed as the temperature is raised above approximately 440°C, due to an increasing rate of desorption of DEGa. This competes with the growth process. Interestingly, the basic scheme agrees with the earlier suggestions of Robertson et al[30], based on a simple, intuitive, theoretical model. Perhaps more importantly, these surface spectroscopy experiments give information useful in understanding more complex problems, such as the rather complex effects of temperature and group III fluxes on the composition of alloys, i.e., GaInAs and AlGaAs[28]. This type of information is also expected to be extremely valuable in the design of new group III precursors for CBE.

## 4. SUMMARY

Thermodynamics acts as the driving force for epitaxial growth and thus places an upper limit on the growth rate. If all of the nutrient phase in the reactor were able to equilibrate with the solid epitaxial layer being grown, the system would be operating at the maximum possible growth rate. This is virtually never the case because of mass transport and surface kinetic limitations. For "normal" epitaxial growth rates and temperatures the surface kinetics are considerably more rapid than diffusion. Thus, most of the vapor phase supersaturation is used to drive the diffusion process. As a result, the vapor phase adjacent to the growing interface is nearly in equilibrium with the solid. This situation allows the construction of a simple model that can be used to accurately predict the solid compositions in III/V alloys in terms of the input vapor pressures and substrate temperature during growth.

The topic of solid immiscibility was also discussed. A large difference in lattice parameter between the end components of a random ternary alloy gives rise to a large positive enthalpy of mixing and a region of solid immiscibility. The growth of metastable alloys was discussed. As an example, metastable

$GaAs_{1-x}Sb_x$ alloys have been grown by OMVPE. The key to growing these metastable alloys is the input V/III ratio. When V/III<1, all of the As and Sb reaching the interface are incorporated. The random As and Sb distribution expected from the random impingement from the vapor phase might be expected to result in a nearly random alloy. However, ordered structures are commonly observed in electron diffraction patterns. The ordering is due to the high strain energy inherent in a random solid alloy consisting of bonds with different preferred lengths. The formation of ordered structures reduces this microscopic strain energy.

The kinetic aspects of epitaxy are by far the most complex and, consequently, the least understood. We are beginning to understand the reactions involved in the homogeneous and heterogeneous pyrolysis of the group III and group V precursors used for VPE. Especially at the high concentrations used in ersatz reactors, these are often complex, involving second order processes such as the attack of the parent molecules by free radicals produced during homolysis. The processes occurring on the surface that lead to growth are even more complex. Both simple bond breaking to produce radicals and radical attack reactions apparently occur heterogeneously. In addition, desorption of parent molecules and intermediates controls the growth rate under certain conditions, as convincingly demonstrated for the CBE growth of GaAs from TEGa and cracked arsine. The motion of steps on the surface and kinks along the step edges also apparently plays a decisive role in the kinetics of VPE processes. Certainly, we expect chemical reactions to be catalyzed at surface steps and kinks. In addition, the selective incorporation of competing atoms at steps and kinks apparently determines the degree of ordering and the specific ordered structures formed during VPE growth.

ACKNOWLEDGEMENTS
The author gratefully acknowledges the financial support of the Department of Energy, the Office of Naval Research, and the Airforce Office of Scientific Research.

REFERENCES
1) J.B. Mullin and D.T.J. Hurle, J. Luminescence 7, 176 (1973); A. Koukitu and H. Seki, Japan. J. Appl. Phys. 23, 74 (1984).
2) G.B. Stringfellow, *Organometallic Vapor Phase Epitaxy: Theory and Practice*, (Academic Press, Boston, 1989), Chapter 3.
3) R.Hekingbottom, C.J. Todd, G.J. Davies, J. Electrochem. Soc. 127, 444 (1980).
4) D. W. Shaw, *Treatise on Solid State Chemistry*, Vol 5, ed., N.B. Hannay (Plenum, New York, 1975) p. 283.
5) See Ref. 2, Chapter 1.
6) G. B. Stringfellow, *Crystal Growth of Electronic Materials*, ed. E. Kaldis (Elsevier Science Publishers B.V., Amsterdam, 1985) p. 247.
7) G. B. Stringfellow, *Semiconductors and Semimetals*, Vol 22, Part A, ed. W. T. Tsang (Academic Press, Inc, Orlando, 1985), p. 209.
8) R. A. Swalin, *Thermodynamics of Solids* (John Wiley and Sons, New York, 1962).

9) G. B. Stringfellow, J. Crystal Growth 27 21 (1974).
10) G. B. Stringfellow, J. Crystal Growth 62 225 (1983).
11) M.J. Cherng, R.M. Cohen and G.B. Stringfellow, J. Electron. Mater. 13, 799 (1984).
12) M.J. Jou and G.B. Stringfellow, J. Crystal Growth 98, 679 (1989).
13) J. R. Pessetto and G. B. Stringfellow, J. Crystal Growth 62 1 (1983).
14) J. Waho, S. Ogawa and S. Maruyama, Japan. J. Appl. Phys. 16 1875 (1977).
15) H. R. Jen, M. J. Cherng, and G. B. Stringfellow, Applied Physics Letters 48, 1603 (1986).
16) G.B. Stringfellow, J. Crystal Growth 98, 108 (1989).
17) D.J. Chadi, J. Vac. Sci. and Technol. A5, 834 (1987).
18) G.S. Chen, D.S. Jaw, and G.B. Stringfellow, J. Appl. Phys. 69, 4263 (1991).
19) G.S. Chen and G.B. Stringfellow, Appl. Phys. Lett. 59, 324 (1991).
20) G.S. Chen and G.B. Stringfellow, Appl. Phys. Lett. 59, 3258 (1991).
21) C.T. Foxon and B.A. Joyce, Surf. Sci. 64, 293 (1977).
22) Reference 2, Chapter 2.
23) S.H. Li, C.A. Larsen, N.I. Buchan, and G.B. Stringfellow, J. Electron. Mater. 18, 457 (1989).
24) S.H. Li, C.A. Larsen, N.I. Buchan, G.B. Stringfellow, W.P. Kosar, and D.W. Brown, J. Appl. Phys. 65, 5161 (1989).
25) S.H. Li, C.A. Larsen, N.I. Buchan, and G.B. Stringfellow, J. Crystal Growth 98, 309 (1989).
26) S.H. Li, N.I. Buchan, C.A. Larsen, and G.B. Stringfellow, J. Crystal Growth 96, 906 (1989).
27) S.P. Watkins and G. Haacke, Appl. Phys. Lett. 59, 2263 (1991).
28) T. Martin and C.R. Whitehouse, J. Crystal Growth 105, 57 (1990).
29) E.M. Gibson, C.T. Foxon, J. Zhang, and B.A. Joyce J. Crystal Growth 105, 81 (1990).
30) A. Robertson, T.H. Chiu, W.T. Tsang, and J.E. Cunningham, J. Appl. Phys. 64, 877 (1988).
31) G.B. Stringfellow J. Crystal Growth (to be published).
32) G.B. Stringfellow J. Crystal Growth 68, 111 (1984).
33) G.B. Stringfellow J. Crystal Growth 70, 133 (1984).
34) See reference 2, Chapter 6.
35) C.B. Cooper, R.R. Saxena, and M.J. Ludowise, J. Electron. Mater. 11 1001 (1982).
36) G.B. Stringfellow and M.J. Cherng, J. Crystal Growth 64 413 (1983).
37) S.H. Li, C.A. Larsen, N.I. Buchan, and G.B. Stringfellow, J. Electron. Mater. 18, 457 (1989).
38) C. Plass, H. heinecke, O. Kayser, H. Luth, and P. Balk, J. Crystal Growth 88, 455 (1988).